

Model guided application for investigating particle number (PN) emissions in GDI spark ignition engines

Author, co-author (Do NOT enter this information. It will be pulled from participant tab in MyTechZone)

Affiliation (Do NOT enter this information. It will be pulled from participant tab in MyTechZone)

Abstract

Model guided application (MGA) combining physico-chemical internal combustion engine simulation with advanced analytics offers a robust framework to develop and test particle number (PN) emissions reduction strategies. The digital engineering workflow presented in this paper integrates the kinetics & SRM Engine Suite with parameter estimation techniques applicable to the simulation of particle formation and dynamics in gasoline direct injection (GDI) spark ignition (SI) engines. The evolution of the particle population characteristics at engine-out and through the sampling system is investigated. The particle population balance model is extended beyond soot to include sulphates and soluble organic fractions (SOF). This particle model is coupled with the gas phase chemistry precursors and is solved using a sectional method. The combustion chamber is divided into a wall zone and a bulk zone and the fuel impingement on the cylinder wall is simulated. The wall zone is responsible for resolving the distribution of equivalence ratios near the wall, a factor that is essential to account for the formation of soot in GDI SI engines. In this work, a stochastic reactor model (SRM) is calibrated to a single-cylinder test engine operated at 12 steady state load-speed operating points. First, the flame propagation model is calibrated using the experimental in-cylinder pressure profiles. Then, the population balance model parameters are calibrated based on the experimental data for particle size distributions from the same operating conditions. Good agreement was obtained for the in-cylinder pressure profiles and gas phase emissions such as NO_x. The MGA also employs a reactor network approach to align with the particle sampling measurements procedure, and the influence of dilution ratios and temperature on the PN measurement is investigated. Lastly, the MGA and the measurements procedure are applied to size-resolved chemical characterisation of the emitted particles.

Introduction

The work presented in this paper is part of the development of particle measurement procedures to lower the current 23 nm limit down to 10 nm for gasoline direct injection (GDI) spark ignition (SI) engines. It entails the fundamental understanding of the particle

formation/loss mechanisms at each stage right from the engine, through the exhaust sampling up to the measurement device. Model guided application comprising detailed physico-chemical models and advanced statistical algorithms has been proposed and developed in order to assist the measurement procedures with the following:

- a) Understanding of the formation and dynamics of the nanoparticles from the source through to sampling up to the measurement instrument.
- b) Sensitivity of the particle size distribution and particle number to the engine operation (e.g., load, speed, etc.) as well as sampling conditions (dilution, temperature, etc.)
- c) Insight into the chemical composition of the particle aggregates.
- d) Calibration of the measurement method which includes the adaptation of a suitable semi-volatile particle removal procedure for the new system.
- e) Data that may be difficult to obtain experimentally, for example, in-cylinder temperature, equivalence ratio distribution, etc.

This paper focuses on the demonstration of the MGA in the context of a single-cylinder GDI SI engine equipped with a wide range of physical and chemical particle characterisation measurement techniques.

Traditional engine calibration methods rely heavily on static tabular relationship between the engine-controlled variables and the corresponding operating points. The extrapolative capability of such methods is usually quite low and experimentalists often have to resort to expensive tests on their engine. It is also worth mentioning that these tests are time consuming compared to the average simulation time. Therefore, this provides the motivation to combine advanced data-driven statistics with adequately detailed yet computationally efficient physico-chemical simulators within the engine development programmes.

Due to the longer ignition delay and higher volatility of gasoline, GDI engines have fewer fuel-rich regions compared to diesel engines especially when the injection takes place long before combustion.

The formation of soot in GDI engines has been investigated through various optical methods such as laser-induced fluorescence (LIF) [1, 2], high-speed camera combustion images [3, 4, 5], laser-induced incandescence (LII) [6, 7], and the two colour method [8]. These studies concluded that there are two main sources of soot formation: the first being locally rich zones and the second pool fires caused by fuel films along the combustion chamber. It was found that soot from the first type of source usually burns out rapidly due to rapid mixing with hot gases and gets oxidised in the flame. Soot particles from the wall film are the ones which persist until late in the cycle.

Particles formed in internal combustion engines can either be solid or liquid condensates. The solid particles are mostly carbonaceous (soot) with some ash content and adsorbed hydrocarbons (or soluble organic fraction (SOF)) on their surfaces. The solid particles are mostly found in the accumulation mode (40 - 1000 nm) although some nucleation mode (7 - 40 nm) particles are typically present. The liquid condensates are either composed of SOF or sulphuric acid and water. These particles tend to be completely in the nuclei mode size class. It is well known that sampling conditions, such as temperature and dilution ratios, can dramatically affect adsorbed SOF and liquid condensates [9].

The vehicle exhaust is a hot and complex mixture with both particulates and gaseous emissions, and it is a standard practice to dilute the exhaust through a sampling line before the measurements. The main concern here is that the particles may undergo processes such as coagulation, condensation and adsorption in the sampling line. Several studies have concluded that a significant fraction of nuclei mode particles is formed in the sampling stage [10, 11, 12] and these particles are believed to be composed of SOF produced when the temperature is low in the sampling line.

There have been several attempts to understand the flow dynamics in the sampling line through the use of computational fluid dynamics (CFD). These studies tend to focus on the formation of sulphuric acid in the sampling system [13, 14]. The major advantage of using a detailed tool such as CFD is that it is possible to identify specific locations in the sampling system that give rise to the nucleation of sulphuric acid and also areas where particles may deposit. However, CFD simulations are known to be computationally expensive and it is not feasible to consider detailed particle formation kinetic schemes such as the ones considered in this work.

The main objective of this paper is to demonstrate a model-based workflow at simulating the in-cylinder gas phase and particulate phase emissions produced in the engine and up to the sampling stage. Two stages are involved in this workflow: i) calibration of the gas phase and particulate phase emissions at engine-out using a physico-chemical model, and ii) investigation of the sampling system with a reactor network model. Figure 1 gives an overview of the different stages considered in this work. The physical system covers the GDI SI engine, the diluter/sampling equipment and the measurement devices. The digital MGA mimics the physical set-up with the help of the physico-chemical SRM Engine Suite, reactor network and analytics. The key outputs from the physical and digital workflows are the particle size distribution (PSD), particle number (PN), particulate mass (PM) and the surface chemical composition of the particles. The physical system and the models are described in detail in the subsequent sections.

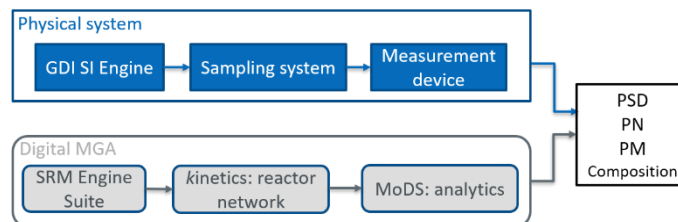


Figure 1: Different stages considered in the simulations before measurement.

Experimental Conditions

Engine

A spark-ignition gasoline fuelled single cylinder research engine with a displacement of 449 cm³ and compression ratio of 12.5 was operated at the range of engine speeds and loads listed in Table 1. In the simulations, only the closed-portion of the cycle is considered. The inlet valve closure (IVC) and exhaust valve opening (EVO) used are -118 CAD aTDC and 116 CAD aTDC respectively.

Table 1: Engine operating conditions

Operating conditions	Engine speed (RPM)	IMEP (bar)
1	1200	2
2	1200	4
3	1200	6
4	1200	8
5	2000	2
6	2000	4
7	2000	6
8	2000	8
9	2500	2
10	2500	4
11	2500	6
12	2500	8

Sampling for particle measurements

The raw exhaust gas was sampled from a port in the exhaust pipe where it is introduced into a Dekati® FPS-4000 for dilution. There are two dilution stages, the first being at a ratio of 2.3:1 with the diluent temperature set to approximately 623 K. The second dilution stage is at ambient temperature and the overall dilution ratio is approximately 30:1. The dilution system is modelled using a network of well-mixed reactors which will be described in the model section.

The diluted exhaust was then fed into a TSI 3090 Engine Exhaust Particle Sizer (EEPS) to measure the particle size distribution (PSD). During an independent sampling campaign using some of the same

engine conditions, a second, parallel line was added in order to collect particles for offline chemical characterisation. The diluted exhaust was introduced into a TSI nanoMOUDI II cascade impactor, which collects particles on 13 size-selected impaction stages. In this study, aluminium foil substrates were installed on the upper stages (nominal cut sizes 10,000 – 10 nm), with one quartz fibre filter as the back filter (<10 nm).

Chemical characterisation of the particles

Time-of-Flight Secondary Ion Mass Spectrometry analysis was conducted with a TOF.SIMS⁵ instrument from ION-TOF GmbH. Briefly, samples were introduced into the analysis chamber which has a residual pressure of $\sim 10^{-9}$ mbar. The sample surface was bombarded by a 25 keV Bi₃⁺ ion beam with a current of 0.3 pA in static mode. Acquisitions were performed for 180 s, with 25 random scans/acquisition used on an area of 500 $\mu\text{m} \times 500 \mu\text{m}$ on the sample surfaces. In this technique, the high energy of the primary ion beam leads to a cascade of collisions between atoms/molecules on the sample surface. Consequently, both neutral and charged (+/-) species are ejected from the sample surface, the latter being called secondary ions. These ions are then extracted and accelerated using ion optics and mass-analysed with a Time-of-Flight tube (V mode) and a detector. For each sample, mass spectra were collected in both positive and negative modes for at least four areas. The mass resolution at m/z 29 was approximately 3500.

Model description

The main focus of this work is to simulate the formation and evolution of particulate emissions from GDI engines. The particulates are mainly formed in the combustion chamber, but it is also important to account for the losses in the sampling line. Hence, the simulations are carried out in two stages. The first stage focuses on the in-cylinder combustion using the SRM that simulates the in-cylinder combustion process as well as the particle formation mechanisms in detail. In the second stage, a reactor network model is used to account for the effects of dilution on the particulates in the sampling system.

Stochastic Reactor Model (SRM)

The SRM is derived from the probability density function (PDF) transport equation. Detailed derivations from first principles and convergence studies have been published previously [15, 16, 17, 18, 19, 20]. The SRM has been used in a variety of applications including the simulation of fuels [21], GDI engines [22, 23, 24, 25, 26], traditional compression ignition engines [27, 28, 29], homogeneous charge compression ignition engines [30, 31, 32, 33], and particulate emissions [34, 35, 36].

The SRM is zero-dimensional, which means that there is no spatial information within the quantities. However, the model does not assume spatial homogeneity, but rather statistical homogeneity. This implies that the PDF is the same everywhere, but the inhomogeneity is described by the distribution represented by the PDF.

The SRM calculates the progression of scalar variables, such as the mass fraction of chemical species Y_1, \dots, Y_{N_S} (N_S denotes the number of chemical species) and temperature T as a function of time t . The random scalar variables can be combined into a vector $\psi = (\psi_1, \dots, \psi_{N_S}, \psi_{N_S+1}) = (Y_1, \dots, Y_{N_S}, T)$, and the joint composition PDF is denoted by $f(\psi; t)$.

In order to account for density variations in the in-cylinder turbulent combustion, it is convenient to apply a mass density function (MDF). The MDF is related to the PDF, and can be written as:

$$\mathcal{F}(\psi; t) \equiv \rho(\psi)f(\psi; t). \quad (1)$$

The MDF transport equation for the SRM can be expressed as follows:

$$\begin{aligned} \frac{\partial}{\partial t} \mathcal{F}(\psi; t) = & - \underbrace{\sum_{j=1}^{N_S+1} \frac{\partial}{\partial \psi_j} [G_j(\psi)\mathcal{F}(\psi; t)]}_{\text{chemical reaction}} + \underbrace{\sum_{j=1}^{N_S+1} \frac{\partial}{\partial \psi_j} [A(\psi)\mathcal{F}(\psi; t)]}_{\text{turbulent mixing}} \\ & - \underbrace{\frac{1}{V} \frac{dV}{dt} \mathcal{F}(\psi; t)}_{\text{piston movement}} - \underbrace{\frac{\partial}{\partial \psi_{N_S+1}} [U(\psi_{N_S+1})\mathcal{F}(\psi; t)]}_{\text{convective heat transfer}} \\ & + \underbrace{\frac{\mathcal{F}_c(\psi; t)}{\tau_{\text{crev}}} - \frac{\mathcal{F}(\psi; t)}{\tau_{\text{cyl}}}}_{\text{crevice flow}} + \underbrace{\frac{\mathcal{F}_f(\psi; t)}{\tau_f}}_{\text{fuel injection}} \end{aligned} \quad (2)$$

where $G_j(\psi)$ and $A(\psi)$ are the operators for chemical reaction and turbulent mixing, V is the sweep volume, $U(\psi_{N_S+1})$ is the heat transfer operator, \mathcal{F}_c and \mathcal{F}_f are the MDFs corresponding to the crevice and fuel injection. The characteristic residence time of in-cylinder gas, crevice gas and fuel are denoted by τ_{cyl} , τ_{crev} and τ_f . The terms on the right-hand side of Equation (2) describe the physical in-cylinder processes of chemical reactions, turbulent mixing, heat transfer, piston movement, crevice flow and fuel injection respectively.

The multi-dimensional MDF transport equation is then solved using a stochastic particle method, in which the MDF is approximated by an ensemble of N_{par} stochastic parcels. In the previous papers, these parcels are referred to as stochastic particles, the term ‘parcel’ is used in this paper to avoid confusion due to the variety of particles involved in the model. Each stochastic parcel is described by a gas phase chemical composition and a temperature, i.e. $\psi^{(i)} = (\psi_1^{(i)}, \dots, \psi_{N_S}^{(i)}, \psi_{N_S+1}^{(i)}) = (Y_1^{(i)}, \dots, Y_{N_S}^{(i)}, T^{(i)})$, where the superscript indices are labels for the parcels. Thus, a parcel is a collection of species mass fraction and a temperature. In addition to these quantities, each parcel contains an additional population of solid particles (mixture of soot and inorganics) and this is described further in the particle model section. In an engine simulation, the gas phase dominates the mass of the parcels and the mass percentage of the solid phase is in the order of 1×10^{-5} %.

An operator splitting technique is used where each of the processes described in Equation (2) acts on the ensemble of stochastic parcels sequentially at each time step (see for example [22]).

Multi-zonal SRM

Three zones are considered in the model: bulk unburned zone, bulk burned zone, and wall zone. The bulk zones form the majority of the in-cylinder charge (99% mass) and the rest of the charge is taken up by the wall zone (1% mass). Each of the zones contains its own ensemble of stochastic parcels. The model remains zero-dimensional, i.e. the parcels do not contain any spatial or geometric information. The three groups of stochastic parcels should be considered as statistical representations of their respective zones.

The main function of the wall zone is to account for the fuel-rich regions along the wall/liner from the impingement of fuel. The size of the wall zone needs to be small in order to produce stochastic parcels with high equivalence ratios whilst ensuring that the bulk zone is close to stoichiometric.

As the focus of this work is on the formation of soot particles from pool fires, the bulk zone is treated as homogeneous for simplification. The level of stratification dictates the number of stochastic parcels required. Since the bulk zone is assumed to be homogeneous, only two parcels are required (one for unburned and one for burned). It is found that having additional parcels in the bulk zone will not affect a homogeneous case because combustion is mainly controlled by the flame speed. As for the wall zone, more stochastic parcels are required to resolve the distribution of equivalence ratios in the fuel-rich zone to simulate the formation of soot accurately. In our current work, it is found that 10 stochastic parcels are sufficient to achieve convergence with the distribution of equivalence ratios considered.

With 2 stochastic parcels in the bulk zone and 10 parcels in the wall zone, a typical simulation from IVC to EVO takes about 30 minutes and may need up to two hours to complete on an 8-core CPU with a clock speed of 3.77 GHz. The majority of the CPU time is spent on computing the rates in the population balance model for particulates.

Flame propagation

Flame propagation only occurs in the bulk zone and is modelled as the growth of the burned zone. At the initiation of the spark, the burned zone obtains its mass from the unburned zone at the flame speed specified by Equation (4). Combustion is simulated in the burned zone by setting its temperature to 2500 K until there is no spark energy left (0.2 J).

The size of the burned zone is determined by the flame and the flame radius at the n^{th} time step, R_n , is obtained from

$$R_n = R_{n-1} + (u_T + S_L)\Delta t \quad (4)$$

where u_T is the characteristic turbulent flame speed [37] and S_L is the laminar flame speed taken from [38]. The turbulent flame speed is defined by

$$u_T = 0.08C_1\bar{u}_{\text{in}}\left(\frac{\rho_u}{\rho_{\text{in}}}\right)^{0.5} \quad (5)$$

where C_1 is the turbulent entrainment constant, \bar{u}_{in} is the mean inlet gas speed, ρ_u is the density of the unburned gas and ρ_{in} is the inlet air density (assumed to be 1.2 kg m^{-3}).

Fuel injection

As the GDI engine considered in this work has very early injection (-270°), it can be safely assumed that the bulk of the cylinder charge is close to stoichiometric and almost homogeneous during combustion. Thus, the main focus is on ensuring that the distribution of equivalence ratios in the wall zone is adequate to simulate pool fires late in the engine cycle.

The equivalence ratio and temperature of the stochastic parcels need to be within the soot region indicated in Figure 2 in order to produce the precursors necessary for the inception of soot particles.

At the beginning of the simulation, a fraction of the incoming fuel is assigned to the wall film in liquid form. Note that the film is not associated with any of the stochastic parcels before evaporation. As the fuel evaporates, the fuel is distributed to the stochastic parcels in the wall zone according to the following distribution profile

$$F^{(i)} = \exp\left(-\alpha\left(\frac{\sum_{l=1}^i m^{(l)}}{\sum_{l=1}^N m^{(l)}}\right)\right). \quad (6)$$

Larger values of α will give more stratified distributions and a value of 0 will give a homogeneous distribution. As the amount of fuel varies for each operating condition, both the evaporation rate and α are tuned case by case accordingly to give a similar behaviour as shown in Figure 2.

Summary of multi-zonal SRM

The MDF, Equation (2), is solved for each zone. The subprocesses (e.g. turbulent mixing and chemical reaction) are solved separately for each zone. The sizes of the bulk unburned and bulk burned zones are controlled by the flame propagation submodel. Tables 2 and 3 summarises the zonal properties and the interaction between the zones.

Table 2: Summary of the zonal properties.

	Mass percentage	Temperature
Bulk unburned	Initialised at 99%. At spark, mass is gradually transferred into the burned zone until it reaches 0%.	300 K to 900 K
Bulk burned	Initialised at 0%. Obtains mass from the unburned zone at spark. Mass will reach approximately 99% at the end of the flame propagation.	1500 K – 2500 K
Wall	Initialised at 1%. Mass will increase slightly from the evaporation of the wall film.	300 K – 1500 K

Table 3: Summary of the interactions between the zones.

	Bulk unburned	Bulk burned	Wall
Bulk unburned	N/A	No mixing. Mass transfer to burned zone during flame propagation	Curl mixing [39]
Bulk burned	No mixing. Mass transfer from the unburned zone during flame propagation.	N/A	Curl mixing [39]

The Curl's mixing model [39] is employed for the mixing between the wall zone and the bulk zones, whereby one stochastic parcel is selected based on their weights from the bulk and wall zones to mix and their compositions are averaged.

To give a clearer picture of the interactions between the zones, the evolution of the stochastic parcels for one of the operating points is demonstrated in Figure 2. Each of the 12 steady-state operating points is calibrated to give a similar behaviour. The actual injection timing used in the experiment is -270 CAD aTDC, but as the SRM only considers the closed-portion of the cycle, fuel is injected at IVC. This does not make any significant difference to the results because most of the fuel has evaporated before the start of combustion.

Figure 2 shows four key phases in the simulation of the SRM Engine Suite. At -30 CAD, most of the injected fuel has evaporated and it can be observed there are two parcels close to stoichiometric and a group of richer parcels. The parcels close to stoichiometric represent the bulk unburned zone (99% mass) and the group of richer parcels represents the wall zone (1% mass in total). At spark, these two unburned parcels are combined to make space for the burned zone. This is purely a computational process and the physical state is unaffected (e.g. pressure, volume etc.) because homogeneity is assumed. It is possible to simulate the first phase with just one parcel in the bulk zone but it will be computationally inconvenient to implement with one empty space in the computational array.

The second phase shows the state of the system slightly after spark, where there are two parcels close to stoichiometric (one burned and one unburned). Combustion is initiated by setting the burned zone temperature to 2500 K. The size of the burned zone grows according to the flame speed.

In the third phase, the wall parcels have gained enough energy from the bulk zone to undergo combustion (pool fires). It can be observed that these parcels are in the soot zone which is conducive to the production of the necessary soot precursors.

The population balance model begins to produce soot in the wall parcels after the third phase. Towards the end of the simulation (fourth phase in Figure 2), it can be observed that significant soot has accumulated in the wall parcels. The inception of soot is modelled as a collision process and the mass of soot incepted in each parcel is proportional to the squared of soot precursor concentration in the gas phase (coronene). In this case, there are two remaining bulk particles near stoichiometric (burned and unburned) which indicates incomplete combustion. The remaining bulk unburned zone has a large contribution to the unburned hydrocarbon (uHC) emissions. Later in the results section, it is shown that good agreement is obtained for the uHC emissions.

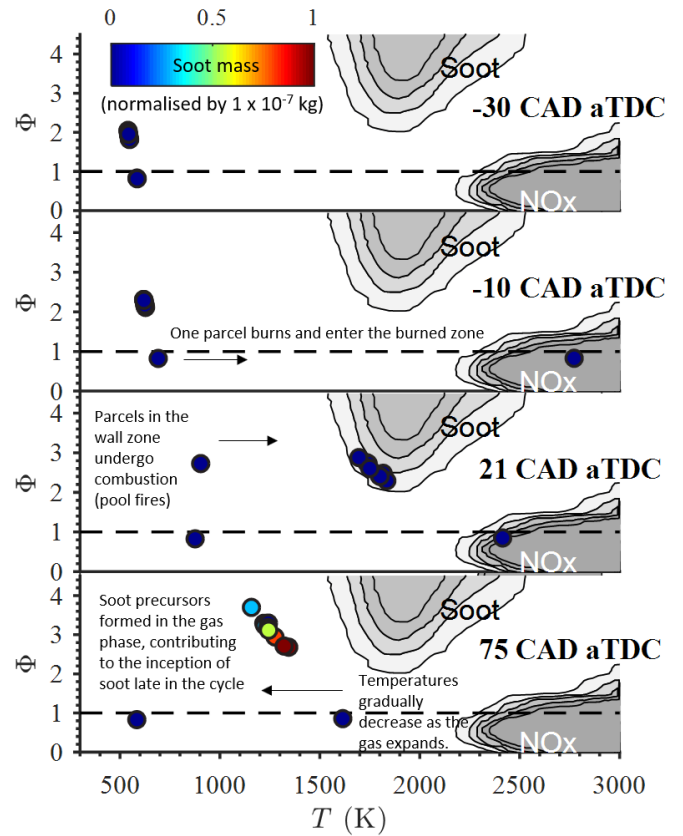


Figure 2: Evolution of phi, temperature, and soot mass of the parcels.

Particle model

A novel population balance model (PBM) is developed to model solid, carbonaceous (soot) particles alongside organic SOF liquid particles. This model is directly coupled with the gas phase chemistry of the SRM Engine Suite. The model considers solid particles containing carbon with SOF compounds condensed on their surfaces. Additionally, the model allows for separate tracking of liquid-like particles composed of SOF compounds. The solid and liquid particles populations can interact with each other via aggregation (coagulation).

The solid particles are represented by three real numbers. A particle $P_{\text{solid},i}$ is given by:

$$P_{\text{solid},i} = P(m, n_p, Y_{\text{SOF}}) \quad (7)$$

where m is the particle's mass, n_p is the number of primaries in the particle, and Y_{SOF} is the mass fraction of SOF compounds in the particle. With this type space, an approximation of the fractal aggregate nature of soot particles can be retrieved [40]. Note that in this model, all primaries within a given particle are assumed to be of equal size. Additionally, there is no information on the connectivity of the primaries within the particle. To retrieve the aggregate structure, the fractal dimension (D_f), fractal pre-factor (k_f), and density of the particles (ρ_p) must be assumed [41].

The liquid particles are represented by a real number. A particle $P_{\text{liquid},i}$ is given by:

$$P_{\text{liquid},i} = P(m). \quad (8)$$

Liquid particles are assumed to be spherical with an assumed density. The processes governing formation and growth of particles in the population balance model include inception, surface growth and oxidation, aggregation (coagulation), and breakage (fragmentation). The PBM is solved via a sectional method [40, 42, 43].

Sampling system

Given the understanding that sampling conditions can greatly affect measurements of particle size distributions due to changes to the amount of absorbed SOF and liquid condensates, there is a need to investigate the effect of the experimental sampling conditions on the predicted PSD and gas phase compositions. To address this concern, the predicted PSDs and gas phase compositions from the SRM Engine Suite are used as input to a simulation of the sampling system. This sampling is modelled using CMCL's kinetics™ software and thus offers the MGA workflow the capability to simulate the gasoline fuel, in-cylinder combustion, emissions at engine-out as well as their evolution through the sampling configuration.

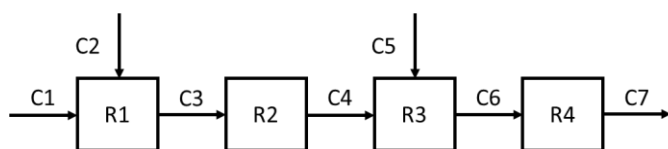


Figure 3: Reactor network in kinetics™ software to represent the sampling system.

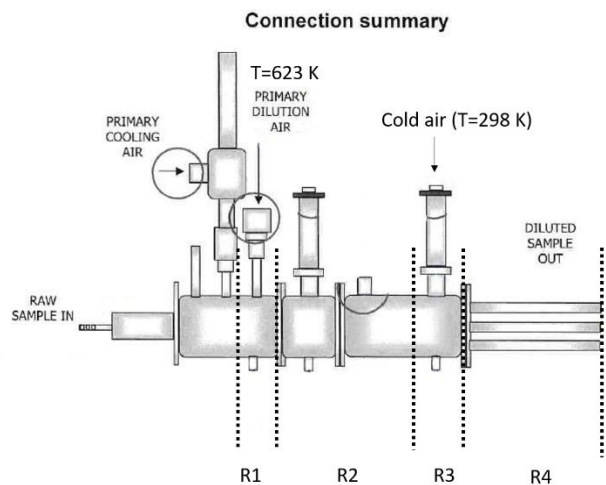


Figure 4: Dekati sampling system [44].

The sampling system is modelled via the reactor network feature in kinetics™. The reactors are specified as constant volume reactors with a volume equal to the physical volume of the piping within the Dekati® FPS-4000. Connections are specified at constant mass flow. Figure 3 shows the reactors and the physical connections between them. The corresponding sections of the sampling system represented by the reactors are also labelled in Figure 4. The first dilution stage is represented by R1 with dilution air at 623 K. The second dilution stage is represented by R3 where there is cold air (298 K) going into the system.

The first connection (C1) represents the inlet to the reactor network at a location just prior to the first dilution stage. The first reactor (R1) represents the first dilution stage assuming a length 40 mm and a diameter of 6 mm. C2 and C4 represents the first and second stage dilution air flow respectively. R2 represents the piping between the first and second dilution stages with a length of 140 mm and a diameter of 6 mm. R3 represents the second dilution stage with the same physical dimensions as R1. Finally, R4 represents the piping for the second dilution stage to the EEPS.

The mass flow rates are calculated based on the EEPS (TSI 3090) manufacturer's specifications for flow rate and temperature of the sampling stream, which are given to be 10 l/min with a temperature range of 283 K to 325 K. Assuming the flow stream has the density of air at 298 K (1.2 g/l) and knowing the dilution ratios (2.3 first stage and 30:1 overall), the mass flows for the connections can be determined (listed in Table 4).

Table 4: Mass flow rates for each connection.

Connection	Mass flow rate (kg/s)
C1	6.35E-06
C2	1.47E-05
C3	2.10E-05
C4	2.10E-05
C5	1.76E-05
C6	1.97E-05
C7	1.97E-05

The temperature of the first and second dilution connections are assumed to be 623 K and 298 K respectively, while the temperature of C1 is assumed to be the average temperature at the end of the SRM Engine Suite simulation for the in-cylinder combustion. The composition for all external connections is assumed to be that of air, except for C1. For this connection, the composition, including the particle population, obtained at the exhaust valve opening from the SRM Engine suite, is used as input with the following modifications. The gas phase composition is reduced to only include species relevant to absorbed SOF and liquid condensate particle formation. The representative SOF species is assumed to be pyrene.

For the solid particles, a loss function to account for ordinary diffusional losses in the sampling system up until the first dilution stage is applied. The loss function is calculated as a function of size, as recommended by Weiden et al [45] and it is shown in Figure 5. Diffusional losses for other parts of the sampling system are not considered as the method in [45] suggests that losses are greatly reduced due to the increased flow rates and reduced temperature after the first dilution stage. Thermophoretic losses are not accounted for due to the reduction in temperature after the dilution stages. Finally, the sulphate formation model is not utilised as predicted engine out SOx levels are too low to support sulphate particle formation. This needs further experimental measurements of SOx in order to confirm the low levels suggested by the MGA.

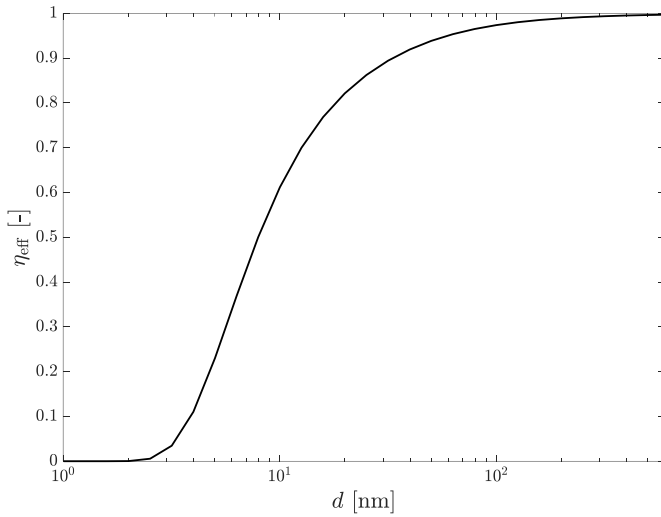


Figure 5: Particle transfer function applied at C1.

Results and Discussions

In-cylinder gas phase (SRM + MoDS)

Figure 6 presents a selection of in-cylinder pressure profiles from the 12 operating conditions. The flame speed, Eq. (4), is calibrated for each operating point with Model Development Suite (MoDS) [46].

To quantify the agreement between the model and experiment, the sum of squares objective function is used:

$$OF = \sum_{i=1}^H (h_i^{\text{sim}} - h_i^{\text{exp}})^2, \quad (9)$$

where h^{sim} denotes the model response, h^{exp} denotes the experimental response and H is the total number of responses considered. For each operating point, 15 points on the pressure curve are included in the objective function.

Optimisation of the objective function is carried out in two stages. The first stage involves a quasi-random global search using a Sobol low-discrepancy sequence [47]. The process begins by defining the boundaries of the model parameter space. Then, Sobol sequences are used to sample the bounded parameter space and the model is evaluated at the generated Sobol points. In the second stage, a local optimisation is carried out from the best Sobol point using the Hooke and Jeeves' algorithm [48].

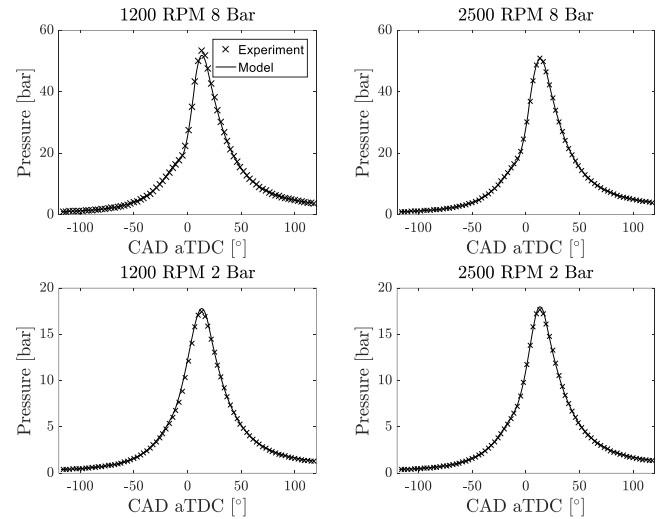


Figure 6: Typical agreement for in-cylinder pressure profiles.

The resulting gas phase emissions (NO_x , unburned hydrocarbons, and CO) from the simulations with the calibrated flame speeds are shown in Figures 7, 8, and 9. NO_x and unburned hydrocarbons are in good agreement. The agreement for CO is not as good as NO_x and uHC but the majority of the simulated values are still within an order of magnitude with the exception of the low load low speed point (1200 RPM 2 bar). The poor agreement for CO may be caused by the assumption that the bulk zone is homogeneous. Since richer conditions are more conducive to the production of CO, it may be necessary to have more stochastic parcels in the bulk zone to have a more resolved distribution of equivalence ratios.

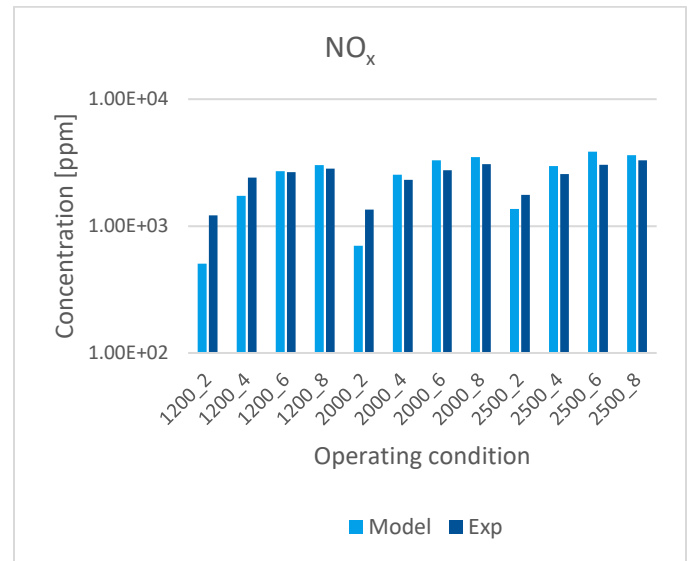


Figure 7: NO_x emissions. (1200_2 denotes 1200 RPM 2 bar, and etc.)

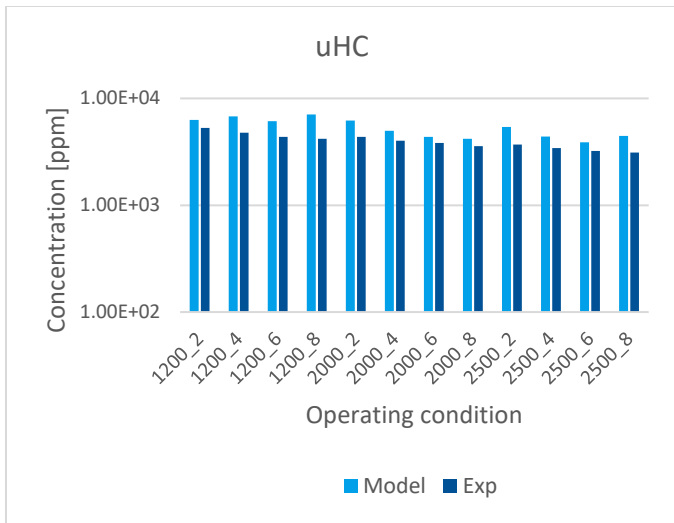


Figure 8: Unburned hydrocarbons emissions. (1200_2 denotes 1200 RPM 2 bar)

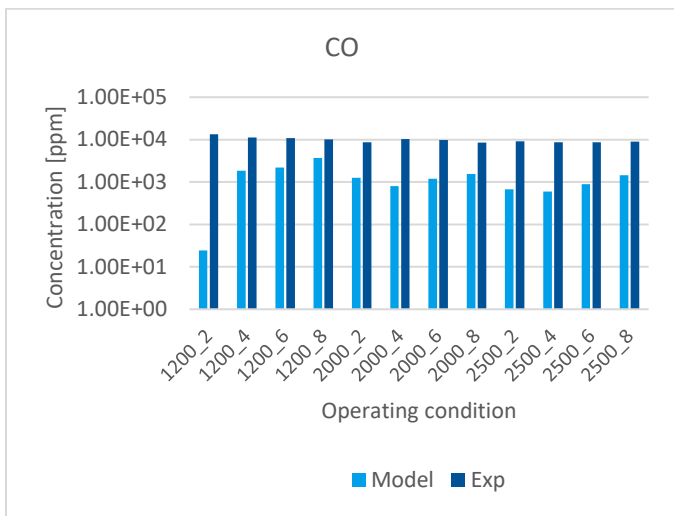


Figure 9: Carbon monoxide emissions. (1200_2 denotes 1200 RPM 2 bar)

In-cylinder particulate phase (SRM)

The majority of the soot particles are formed in the wall zone because only the stochastic parcels in the wall zone are rich enough to produce the necessary soot precursors (coronene) – see Figure 2. The calibration of the particulate phase is almost independent from the gas phase (flame propagation) as the wall zone only occupies 1% mass of the charge.

Due to the sensitivity of the PBM parameters and the huge uncertainties shown in the experimental measurements, these parameters were calibrated manually instead of using MoDS. The sensitivity of the parameters makes it difficult to define suitable bounds on the parameters and the uncertainties in the experimental measurements make it challenging to define a suitable objective function.

Figure 10 presents a selection of calibrated aggregate size distributions from the SRM Engine Suite compared to the measured particle size distributions. The upper and lower bounds in the figure Page 8 of 14

represent the minimum and maximum values measured by the EEPS over ten minutes. There are certain size classes without lower bounds and they represent points with zero as their minimum value. It can be observed from the experimental data that the variability of the particle number increases with engine speed.

Please note that the results are presented on a log-log scale. On a linear scale, the disagreement for the larger particles sizes for some of the cases would not be noticeable; however, a log-log scale is chosen so that the entire distribution can be compared. Additionally, since the peak of the distribution for all cases is well reproduced, the number of particles (PN) is well reproduced as well. Given the state of the art, this is considered an excellent result, as most modelling efforts cannot reproduce even the correct order of magnitude for PN. The PN emissions for all the calibrated operating points are shown in Figure 11.

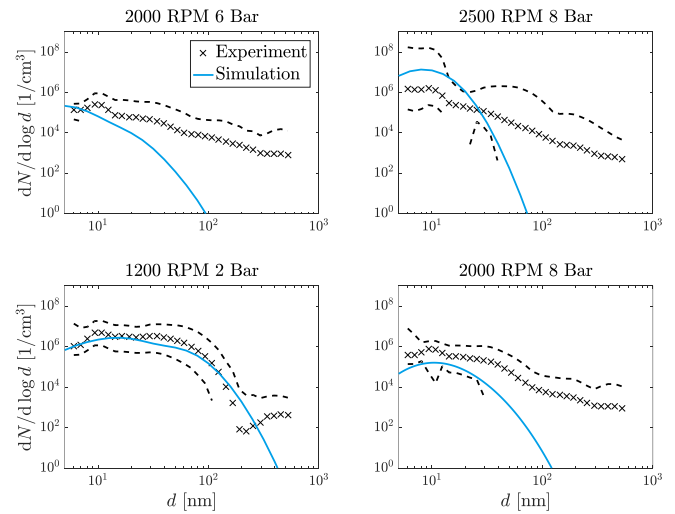


Figure 10: Aggregate size distributions for a selection of operating points.

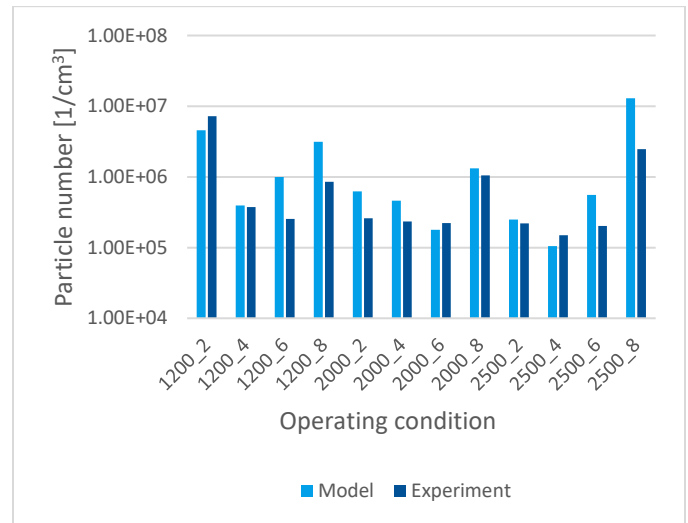


Figure 11: Total particle number for all the operating points.

Sampling system (kinetics™)

Figure 12 shows the temperature at each stage in the reactor network for the operating point 2000 RPM 8 bar. It is assumed that there is no heat loss to the surroundings and the mixture in each reactor is homogeneous. At this point, this assumption is made to simplify the model. As there are no barriers between the different stages, the overall temperature in the sampling system is more homogeneous compared to the step changes depicted in Figure 12. If a detailed flow field is required, then it will be more suitable to use a tool such as CFD. However, it will be challenging to couple the PBM used in this work to CFD and CFD simulations are computationally more expensive to run compared to the reactor network model, thus making it less feasible to perform sensitivity analyses. The temperature at C1 represents the temperature at EVO from the SRM Engine Suite. The exact temperature of C1 changes for each operating point but the overall properties of the reactor network do not vary significantly. It can be observed that the temperature decreases in two stages and this corresponds to the first and second dilution stages (R1 and R3).

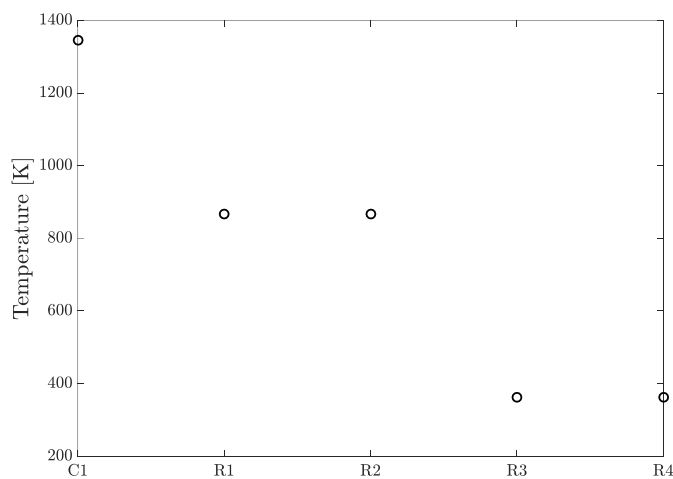


Figure 12: Temperature at each stage in the reactor network.

Figure 13 shows the evolution of the aggregate size distribution through the sampling system modelled in kinetics™. The blue line labelled 'Engine out' represents the aggregate size distribution simulated by the SRM Engine Suite. These particles contain solids only and do not contain any SOF condensates as the temperature at this stage is still high.

The aggregate size distribution shown by R1 shows the effects of applying the loss function shown in Figure 5 and the slight dilution (2.3:1) in the first stage. The loss function removes the majority of the smaller particles and the dilution reduces the overall concentration slightly. R4 shows the aggregate size distribution after the entire reactor network.

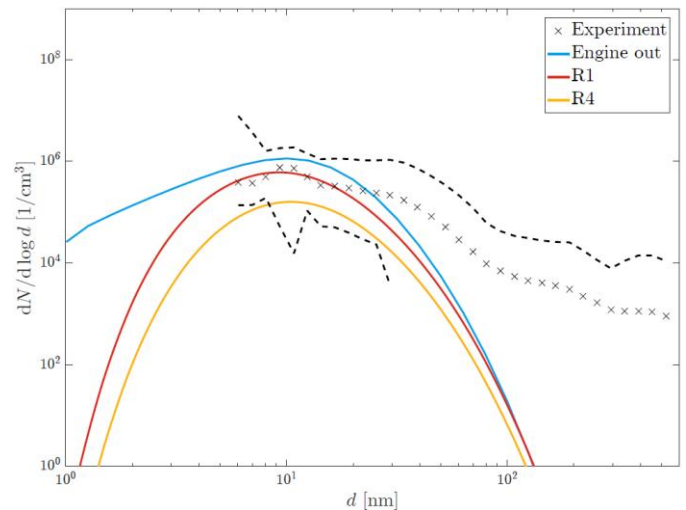


Figure 13: Evolution of particle size distribution through the dilution system.

Figure 14 shows the SOF mass fraction of the aggregates as a function of size along the reactor network. As the temperatures in R1 and R2 are still too high for the condensation of SOF, there is no condensation of SOF until R3 and R4.

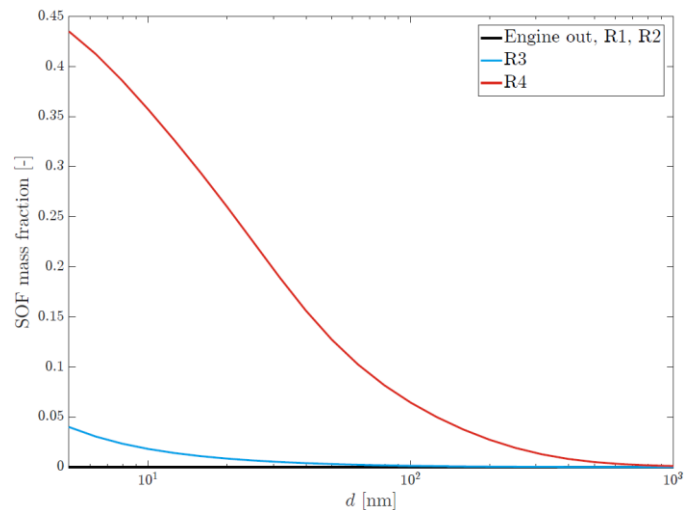


Figure 14: SOF mass fractions as a function of particle size at each stage.

Figure 15 shows how kinetics™ can be used to assess the performance of the sampling system. As opposed to carrying out costly experiments, a single evaluation of this reactor network model only takes less than a minute. This makes it straightforward to carry out a wide variety of sensitivity analyses on the system. For example, the user of the Dekati sampling system may want to investigate the effects of different pipe lengths for transferring the diluted sample to the measurement device. For a preliminary investigation, the user may run the reactor network model by varying the volume of R4 (see Figure 3).

Here, we give an example of such a sensitivity analysis where the effects of the dilution ratio on the sampling system are investigated. It has been established that the particulates in the hot vehicle exhaust are transformed differently during the dilution stage before measurement [10]. In the sampling system, particles may undergo

processes such as coagulation and adsorption, and these are simulated in the reactor network. Based on the tests performed, it is necessary to increase the dilution ratio in multiples of two in order to observe significant reduction in the amount of SOF adsorbed on the particles. Due to the lack of data, it cannot be ascertained that the simulated SOF mass fractions are representative of the conditions in the measurements. However, this demonstrates the potential of the MGA to serve as a guidance to experimentalists on the performance of their setup.

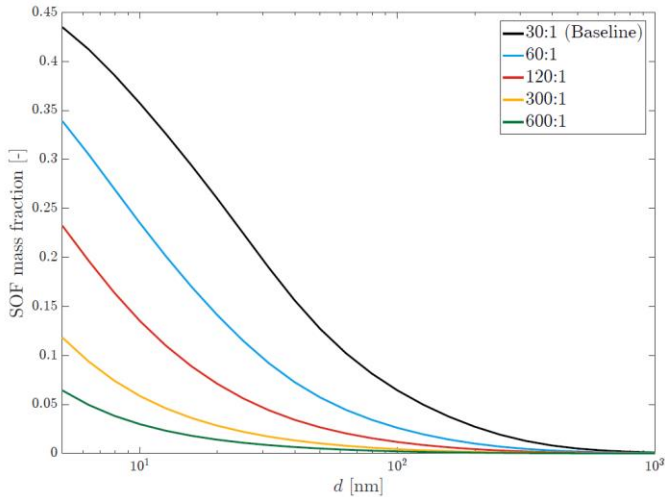


Figure 15: SOF mass fractions for a range of dilution ratios.

Size-resolved particle characterisation (kinetics™)

Mass spectra were normalised to the total ion count (TIC) and further analysed to determine and categorise the surface chemical composition of the samples. All detected mass peaks were assigned to one of four categories: organic compounds, elemental carbon, ash, and sulphur-bearing compounds [49]. Organic compounds are defined as all the organic species (aromatic or aliphatic molecules and their fragments) that are detected in the positive polarity spectra. Carbon clusters C_n^- are considered to be a marker for elemental carbon [49, 50, 51] and form the second group. All the inorganic species, with the exception of sulphur-bearing compounds, were interpreted as ash (metals). Only a few compounds containing sulphur were detected in these analyses, namely: SO_3^- , SO_4^- , HSO_3^- and HSO_4^- . For each category, the areas of all mass peaks were calculated and summed to obtain a representative value of each group's overall contribution [49]; the standard deviation was calculated from the values obtained in different zones of the same example. The results are presented in Figure 16. The total ion count is plotted against the upper bounds of the different TSI nanoMOUDI impactor stages which correspond to particle size. The samples for this study were taken from the operating point 2000 RPM 6 bar.

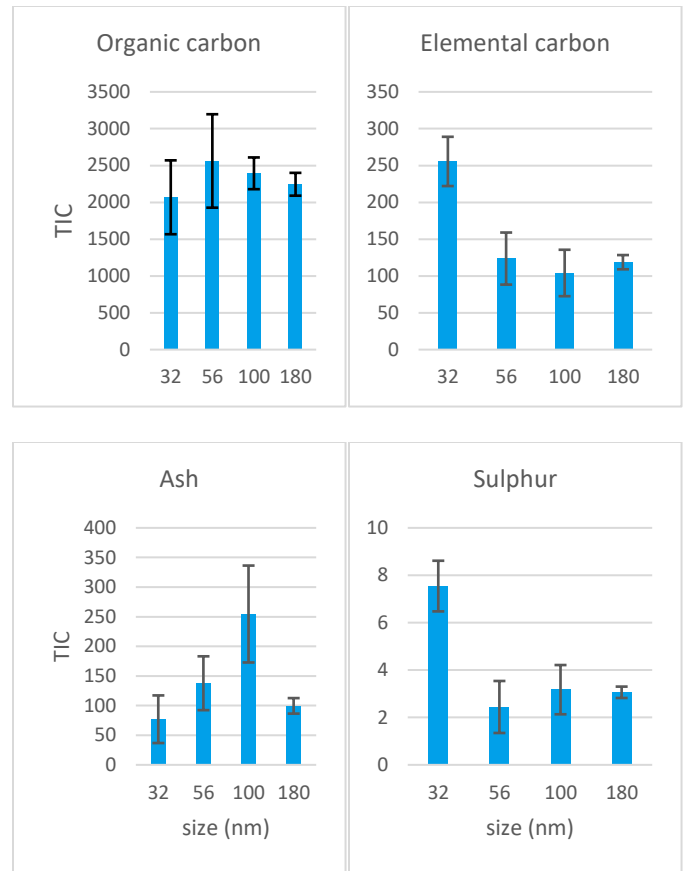


Figure 16: TIC as a function of size.

For comparison with the model, the main focus is on the organic compounds for a couple of reasons. Firstly, the mass spectrometry analysis is a surface characterisation, so the results may not be representative of the particles' bulk composition. Secondly, the model accounts for the condensation of SOF on the soot particles, hence, comparing the thickness of the SOF layer with the results for organic compounds is the best way to utilise the experimental data. Lastly, although the PBM is capable of simulating the formation of sulphuric acid, the sulphur content in the fuel is negligibly low to allow any meaningful comparison.

Figure 17 shows the chemical characteristics of the simulated particles at the end of the sampling reactor network for the operating point 2000 RPM 6 bar. Similar trends are observed for the other operating points. The trend shown by the SOF layer thickness matches the trend shown by the organic carbon mass spectra. The condensation of SOF in the PBM is roughly proportional to the section's concentration. Therefore, the section with the highest number density will obtain the most soluble organics and this corresponds to the peaks shown in total SOF mass and SOF layer thickness in Figure 17. Furthermore, the number of primaries is an indication of the total surface area of the aggregates. As the number of primaries increases with size, significantly more SOF is required to coat the particles to achieve a certain level of thickness.

In this section, the model is validated by comparing the SOF layer thickness with the experimentally measured organic carbon content. The results confirmed that surface composition is not a measure of bulk characteristics. This is further supported by the decreasing carbon trend shown in the mass spectra as it has been concluded that

the nuclei mode particles should have higher SOF [10, 11, 12]. Besides that, the simulated soot mass fractions are also in agreement with the general trend agreed in the literature (SOF mass fraction = 1 – soot mass fraction). Understanding the chemical composition of the particles is important to validate the mechanisms considered in detailed particle models such as the one used in this work and the development of detailed particle models helps us to predict engine emissions better.

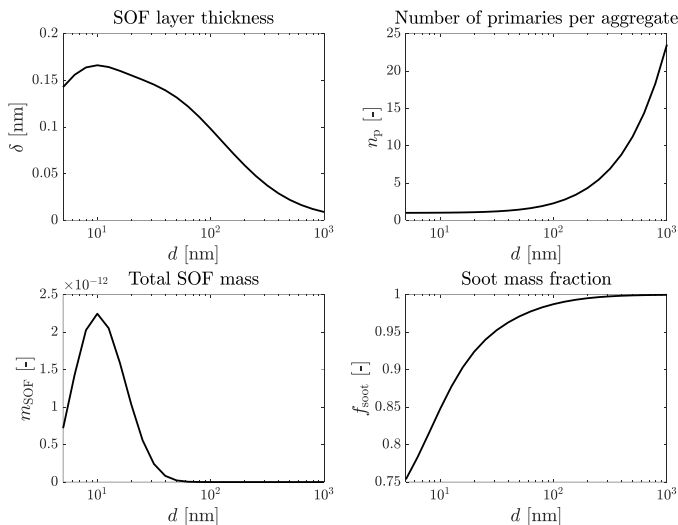


Figure 17: Simulated size-resolved particle characterisation.

Conclusions

Model Guided Application (MGA) comprising physico-chemical simulation and advanced statistics has been formulated as part of the development of measurement procedures to robustly detect emitted particles down to sizes as small as 10 nm. The digital engineering workflow simulates the formation of particles in a gasoline direct injection (GDI) spark ignition (SI) engine generated from combustion as well as fuel wall-impingement, as well as the evolution of the particle population through the exhaust sampling system. In addition to the physical characterisation of particles, size-resolved chemical characterisation is also performed with measurements and with MGA, and compared.

The results in this paper demonstrate the ability to use a model-based framework to assess the performance of an experimental setup as well as the nature of the experimental data. For example, a range of dilution ratios was investigated for the sampling system and the results indicate the threshold for the dilution ratios that is necessary to reduce the amount of soluble organic fraction (SOF) adsorbed on the particles in the sampling stage.

Furthermore, the surface characterisation of organic carbon using the mass spectrometry analysis and the SOF layer thickness (the model accounts for the condensation of SOF on soot) tracked by the digital engineering workflow indicate that the surface composition of a particle is not a measure of its bulk characteristics.

References

- [1] D. W. Stanton and C. J. Rutland, "Modeling Fuel Film Formation and Wall Interaction in Diesel Engines," *SAE Technical Paper 960628*, 1996.
- [2] R. Ortman, S. Arndt, J. Raimann, R. Grzeszik and G. Würfel, "Methods and Analysis of Fuel Injection, Mixture Preparation and Charge Stratification in Different Direct Injected SI Engines," *SAE Technical Paper 2001-01-0970*, 2001.
- [3] F. Catapano, S. D. Iorio, M. Lazzaro, P. Sementa and B. M. Vaglieco, "Characterization of Ethanol Blends Combustion Processes and Soot Formation in a GDI Optical Engine," *SAE Technical Paper 2013-01-1316*, 2013.
- [4] M. Fatouraie, M. Wooldridge and S. Wooldridge, "In-Cylinder Particulate Matter and Spray Imaging of Ethanol/Gasoline Blends in a Direct Injection Spark Ignition Engine," *SAE International Journal of Fuels and Lubricants*, vol. 6, no. 1, pp. 1-10, 2013.
- [5] L. P. Wyszynski, R. Aboagye, R. Stone and G. Kalghatgi, "Combustion Imaging and Analysis in a Gasoline Direct Injection Engine," *SAE Technical Paper 2004-01-0045*, 2004.
- [6] A. Velji, K. Yeom, U. Wagner, U. Spicher, M. Rossbach, R. Suntz and H. Bockhorn, "Investigations of the Formation and Oxidation of Soot Inside a Direct Injection Spark Ignition Engine Using Advanced Laser-Techniques," *SAE Technical Paper 2010-01-0352*, 2010.
- [7] J. N. Geiler, R. Grzeszik, S. Quaing, A. Manz and S. A. Kaiser, "Development of laser-induced fluorescence to quantify in-cylinder fuel wall films," *International Journal of Engine Research*, vol. 19, no. 1, pp. 134-147, 2018.
- [8] B. D. Stojkovic, T. D. Fansler, M. C. Drake and Volker Sick, "High-speed imaging of OH* and soot temperature and concentration in a stratified-charge direct-injection gasoline engine," *Proceedings of the Combustion Institute*, vol. 30, no. 2, pp. 2657-2665, 2005.
- [9] D. B. Kittelson, "Engines and nanoparticles: a review," *Journal of Aerosol Science*, vol. 29, no. 5 - 6, pp. 575 - 588, 1998.
- [10] M. M. Maricq, R. E. Chase, D. H. Podsiadlik and R. Vogt, "Vehical Exhaust Particle Size Distributions: A Comparison of Tailpipe and Dilution Tunnel Measurements," *SAE Technical Paper 1999-01-1461*, 1999.
- [11] T. Kawai, Y. Goto and M. Odaka, "Influence of Dilution Process on Engine Exhaust Nano-Particles," *SAE Technical Paper 2004-01-0963*, 2004.
- [12] E. Vouitsis, L. Ntziachristos and Z. Samaras, "Modelling of diesel exhaust aerosol during laboratory sampling," *Atmospheric Environment*, vol. 39, no. 7, pp. 1335-1345, 2005.
- [13] M. Olin, T. Rönkkö and M. D. Maso, "CFD modeling of a vehicle exhaust laboratory sampling system: sulfur-driven

nucleation and growth in diluting diesel exhaust,” *Atmospheric Chemistry and Physics*, vol. 15, pp. 5305-5323, 2015.

- [14] T. Wey and N.-S. Liu, “Modeling Jet Engine Aerosols in the Postcombustor Flow Path and Sampling System,” *Journal of Propulsion and Power*, vol. 23, no. 5, pp. 930-941, 2007.
- [15] M. Kraft, P. Maigaard, F. Mauss, M. Christensen and B. Johansson., “Investigation of combustion emissions in a homogeneous charge compression injection engine: Measurements and a new computational model,” *Proceedings of the Combustion Institute*, vol. 28, no. 1, pp. 1195-1201, 2000.
- [16] M. Balthasar, F. Mauss, A. Knobel and M. Kraft, “Detailed modeling of soot formation in a partially stirred plug flow reactor,” *Combustion and Flame*, vol. 128, no. 4, pp. 395-409, 2002.
- [17] P. Maigaard, F. Mauss and M. Kraft, “Homogeneous charge compression ignition engine: A simulation study on the effects of inhomogeneities,” *Journal of engineering for gas turbines and power*, vol. 125, no. 2, pp. 466-471, 2003.
- [18] A. Bhave, M. Balthasar, M. Kraft and F. Mauss, “Analysis of a natural gas fuelled homogeneous charge compression ignition engine with exhaust gas recirculation using a stochastic reactor model,” *The International Journal of Engine Research*, vol. 5, no. 1, pp. 93-104, 2004.
- [19] A. Bhave and M. Kraft, “Partially stirred reactor model: analytical solutions and numerical convergence study of a PDF/Monte Carlo Method,” *SIAM Journal on Scientific Computing*, vol. 25, no. 1, pp. 1798-1823, 2004.
- [20] A. Bhave, M. Kraft, L. Montorsi and F. Mauss, “Sources of CO emissions in an HCCI engine: A numerical analysis,” *Combustion and Flame*, vol. 144, pp. 634-367, 2006.
- [21] N. Morgan, A. Smallbone, A. Bhave, M. Kraft, R. Cracknell and G. Kalghatgi, “Mapping surrogate gasoline compositions into RON/MON space,” *Combustion and Flame*, vol. 157, pp. 1122-1131, 2010.
- [22] J. E. Etheridge, S. Mosbach, M. Kraft, H. Wu and N. Collings, “Modelling cycle to cycle variations in an SI engine with detailed chemical kinetics,” *Combustion and Flame*, vol. 158, pp. 179-188, 2011.
- [23] J. E. Etheridge, S. Mosbach, M. Kraft, H. Wu and N. Collings, “Modelling soot formation in a DISI engine,” *Proceedings of the Combustion Institute*, vol. 33, pp. 3159-3167, 2011.
- [24] J. E. Etheridge, A. Bhave, A. R. Coble, A. J. Smallbone, S. Mosbach and M. Kraft, “Optimisation of injection strategy, combustion characteristics and emissions for IC engines using advanced simulation technologies,” *SAE Technical Paper 2011-26-0080*, 2011.
- [25] J. Etheridge, S. Mosbach, M. Kraft, H. Wu and N. Collings, “A detailed chemistry simulation of the SI-HCCI transition,” *SAE International Journal of Fuels and Lubricants*, vol. 3, pp. 230-240, 2010.
- [26] J. Etheridge, S. Mosbach, M. Kraft, H. Wu and N. Collings, “A Fast Detailed-Chemistry Modelling Approach for Simulating the SI-HCCI Transition,” *SAE Technical Paper 2010-01-1241*, 2010.
- [27] A. Smallbone, A. Bhave, M. Hillman, A. Saville and R. McDavid, “Virtual Performance and Emissions Mapping for Diesel Engine Design Optimization,” *SAE Technical Paper 2013-01-0308*, 2013.
- [28] A. Smallbone, A. Bhave, A. R. Coble, S. Mosbach, M. Kraft and R. McDavid, “Identifying Optimal Operating Points in Terms of Engineering Constraints and Regulated Emissions in Modern Diesel Engines,” *SAE Technical Paper 2011-01-1388*, 2011.
- [29] J. Lai, O. Parry, S. Mosbach, A. Bhave and V. Page, “Evaluating Emissions in a Modern Compression Ignition Engine Using Multi-Dimensional PDF-Based Stochastic Simulations and Statistical Surrogate Generation,” *SAE Technical Paper 2018-01-1739*, 2018.
- [30] S. Mosbach, H. Su, M. Kraft, A. Bhave, F. Mauss, Z. Wang and J. X. Wang, “Dual injection homogeneous charge compression ignition engine simulation using a stochastic reactor model,” *International Journal of Engine Research*, vol. 8, no. 1, pp. 41-50, 2007.
- [31] J. Etheridge, S. Mosbach, M. Kraft, H. Wu and N. Collings, “A Detailed Chemistry Multi-cycle Simulation of a Gasoline Fueled HCCI Engine Operated with NVO,” *SAE International Journal of Fuels and Lubricants*, vol. 2, no. 1, pp. 13-27, 2009.
- [32] L. Cao, H. Su, S. Mosbach, A. Bhave, M. Kraft, A. Dries and R. M. McDavid, “Influence of Injection Timing and Piston Bowl Geometry on PCCI Combustion and Emissions,” *SAE International Journal of Engines*, pp. 1019-1033, 2009.
- [33] S. Mosbach, A. M. Aldawood and M. Kraft, “Real-Time Evaluation of a Detailed Chemistry HCCI Engine Model Using a Tabulation Technique,” *Combustion Science and Technology*, vol. 180, no. 7, pp. 1263-1277, 2008.
- [34] A. Smallbone, A. Bhave, A. Coble, S. Mosbach, M. Kraft, N. Morgan and G. Kalghatgi, “Simulating PM Emissions and Combustion Stability in Gasoline/Diesel Fuelled Engines,” *SAE Technical Paper 2011-01-1184*, 2011.
- [35] S. Mosbach, M. S. Celnik, A. Raj, M. Kraft, H. R. Zhang, S. Kubo and K.-O. Kim, “Towards a detailed soot model for internal combustion engines,” *Combustion and Flame*, vol. 156, no. 6, pp. 1156-1165, 2009.

- [36] D. Kittelson and M. Kraft, "Particle Formation and Models," in *Encyclopedia of Automotive Engineering*, 2015, pp. 1-23.
- [37] J. C. Keck, "Turbulent flame structure and speed in spark-ignition engines," *Symposium (International) on Combustion*, vol. 19, no. 1, pp. 1451-1466, 1982.
- [38] J. Heywood, *Internal Combustion Engine Fundamentals*, New York: McGraw-Hill, 1988.
- [39] R. L. Curl, "Dispersed phase mixing: I. Theory and effects in simple reactors," *AIChE Journal*, vol. 9, pp. 175-181, 1963.
- [40] N. Eaves, Q. Zhang, F. Liu, H. Guo, S. Dworkin and M. Thomson, "CoFlame: A refined and validated numerical algorithm for modeling sooting laminar coflow diffusion flames," *Computer Physics Communications*, vol. 207, pp. 464-477, 2016.
- [41] Q. Zhang, H. Guo, F. Liu, G. Smallwood and M. Thomson, "Modeling of soot aggregate formation and size distribution in a laminar ethylene/air coflow diffusion flame with detailed PAH chemistry and an advanced sectional aerosol dynamics model," *Proceedings of the Combustion Institute*, vol. 32, pp. 761-768, 2009.
- [42] N. Eaves, S. Dworkin and M. Thomson, "The importance of reversibility in modeling soot nucleation and condensation processes," *Proceedings of the Combustion Institute*, vol. 35, pp. 1787-1794, 2015.
- [43] N. Eaves, S. Dworkin and M. Thomson, "Assessing relative contributions of PAHs to soot mass by reversible heterogeneous nucleation and condensation," *Proceedings of the Combustion Institute*, vol. 36, pp. 935-945, 2017.
- [44] Dekati, "FPS User Manual," 2010.
- [45] S.-L. v. d. Weiden, F. Drewnick and S. Borrmann, "Particle Loss Calculator – a new software tool for the assessment of the performance of aerosol inlet systems," *Atmospheric Measurement Techniques*, vol. 2, pp. 479-494, 2009.
- [46] CMCL Innovations, "MoDS (Model Development Suite)," 2018. [Online]. [Accessed 2018].
- [47] I. M. Sobol, "On the Systematic Search in a Hypercube," *SIAM Journal on Numerical Analysis*, vol. 16, no. 5, pp. 790-793, 1979.
- [48] R. Hooke and T. A. Jeeves, "Direct Search" solution of numerical and statistical," *Journal of the ACM*, vol. 8, no. 2, pp. 212-229, 1961.
- [49] J. Pagels, D. D. Dutcher, M. R. Stolzenburg, P. H. McMurry, M. E. Gälli and D. S. Gross, "Fine-particle emissions from solid biofuel combustion studied with single-particle mass spectrometry: Identification of markers for organics, soot, and ash components," *Journal of Geophysical Research: Atmospheres*, vol. 118, pp. 859-870, 2013.
- [50] U. Kirchner, R. Vogt, C. Natzeck and J. Goschnick, "Single particle MS, SNMS, SIMS, XPS, and FTIR spectroscopic analysis of soot particles during the AIDA campaign," *Journal of Aerosol Science*, vol. 34, no. 10, pp. 1323-1346, 2003.
- [51] O. B. Popovicheva, C. Irimiea, Y. Carpentier, I. K. Ortega, E. D. Kireeva, N. K. Shonija, J. Schwarz, M. Vojtíšek-Lom and C. Focsa, "Chemical composition of diesel/biodiesel particulate exhaust by FTIR spectroscopy and mass spectrometry: Impact of fuel and driving cycle," *Aerosol and Air Quality Research*, vol. 17, no. 7, pp. 1717-1734, 2017.

Contact Information

Dr Amit Bhave (anbhave@cmclinnovations.com)

CMCL Innovations,

Sheraton House, Castle Park,

CB3 0AX Cambridge

United Kingdom.

Acknowledgement

This work was supported by the H2020 project PEMs4Nano Grant Agreement No. 724145.

Definitions/Abbreviations

aTDC	After top dead centre
CAD	Crank angle degrees
CFD	Computational fluid dynamics
EEPS	Engine exhaust particle sizer
EVO	Exhaust valve opening
GDI	Gasoline direct injection.
IMEP	Indicated mean effective pressure
IVC	Inlet valve closure
LIF	Laser-induced fluorescence

LII	Laser-induced incandescence	PSD	Particle size distribution
MDF	Mass density function	RPM	Rotation per minute
MGA	Model guided application	SOF	Soluble organic fraction
PBM	Population balance model	SRM	Stochastic reactor model
PDF	Probability density function	TIC	Total ion count
PN	Particle number	uHC	Unburned hydrocarbons